Frontiers in Bioscience Landmark

Front. Biosci. (Landmark Ed) **2026**; 31(4): 49564
https://doi.org/10.31083/FBL49564

Original Research

Platelet Factor 4: A Novel Therapeutic Inhibitor for Experimental Neovascular Age-Related Macular Degeneration

Xiubin Ke[1], Shuqi Liang[2], Tianhao Qu[1], Shenyu Li[1], Ji Lei[1], Han Han[1], Yingying Guo[3], Man Xing[3], Xiaohong Wang[1,4], Shikun He[5], Mengyu Liao[1,4], Dongming Zhou[3,*], Hua Yan[1,2,*]

[1]Department of Ophthalmology, Tianjin Medical University General Hospital, International Joint Laboratory of Ocular Diseases (Ministry of Education), State Key Laboratory of Experimental Hematology, Tianjin Key Laboratory of Ocular Trauma, Laboratory of Molecular Ophthalmology, Tianjin Medical University, 300070 Tianjin, China
[2]Department of Clinical Medicine, School of Medicine, Nankai University, 300071 Tianjin, China
[3]School of Basic Medical Sciences, Tianjin Medical University, 300070 Tianjin, China
[4]Department of Pharmacology, Tianjin Key Laboratory of Inflammation Biology, School of Basic Medical Sciences, Tianjin Medical University, 300070 Tianjin, China
[5]Department of Pathology and USC Roski Eye Institute, Keck School of Medicine of the University of Southern California, Los Angeles, CA 90033, USA
*Correspondence: zhoudongming@tmu.edu.cn (Dongming Zhou); zyyyanhua@tmu.edu.cn (Hua Yan)
Academic Editor: Dario Rusciano
Submitted: 30 December 2025 Revised: 12 March 2026 Accepted: 27 March 2026 Published: 23 April 2026

Abstract

Background: Platelet factor 4 (PF4/CXCL4) is a chemokine with reported anti-angiogenic and immunomodulatory properties; however, the role of PF4 in neovascular age-related macular degeneration (nAMD) remains unclear. Thus, this study aimed to evaluate the therapeutic potential of PF4 in experimental models of ocular pathological neovascularization and explored the underlying mechanisms. **Methods**: PF4 expression was assessed in a laser-induced choroidal neovascularization (CNV) mouse model using quantitative real-time PCR (qRT-PCR), enzyme-linked immunosorbent assay (ELISA), and immunofluorescence. Recombinant PF4 was administered intravitreally in laser-induced CNV mice and very low-density lipoprotein receptor knockout ($Vldlr^{-/-}$) mice, a model of spontaneous retinal neovascularization with retinal angiomatous proliferation (RAP)-like lesions. Pathological neovascularization and vascular leakage were quantified by fundus fluorescein angiography and choroidal/retinal flat-mount analyses. Immunofluorescence, qRT-PCR, and RNA sequencing were employed to evaluate inflammatory responses. Moreover, the effects of PF4 on vascular endothelial growth factor (VEGF)-induced proliferation, migration, and tube formation of human retinal microvascular endothelial cells were examined *in vitro*, and VEGF-mediated signaling was analyzed by Western blotting. Ocular safety was assessed by optical coherence tomography (OCT), electroretinography (ERG), hematoxylin and eosin (H&E) staining, and terminal deoxynucleotidyl transferase dUTP nick end labeling (TUNEL) assay. **Results**: Intravitreal PF4 significantly reduced pathological neovascularization and vascular leakage in both models and attenuated intraocular inflammation, as indicated by decreased expression of proinflammatory cytokines and reduced microglial/macrophage recruitment. PF4 inhibited VEGF-induced endothelial cell proliferation, migration, and tube formation *in vitro*. Mechanistically, PF4 downregulated VEGF expression in CNV lesions *in vivo* and suppressed VEGF-induced activation of vascular endothelial growth factor receptor 2 (VEGFR2) and downstream extracellular signal-regulated kinase (ERK), protein kinase B (AKT), and signal transducer and activator of transcription 3 (STAT3) signaling *in vivo* and *in vitro*. PF4 administration was well tolerated, with no detectable adverse effects on retinal structure or function. **Conclusions**: PF4 effectively inhibits ocular pathological neovascularization and inflammation by modulating the VEGF/VEGFR2 signaling pathway. These findings support PF4 as a promising therapeutic candidate for nAMD and warrant further investigation.

Keywords: platelet factor 4; wet macular degeneration; neovascularization; pathologic; choroidal neovascularization; inflammation

1. Introduction

Age-related macular degeneration (AMD) is a leading cause of irreversible vision loss in the elderly worldwide [1]. It primarily manifests in two forms: the more prevalent dry (atrophic) type and the less common but visually more devastating wet (neovascular) form [2]. Neovascular AMD (nAMD) is characterized by pathological neovascularization; these aberrant vessels are prone to leakage, hemorrhage, and eventual fibrotic scarring, leading to rapid and severe central vision loss [3].

The pathogenesis of nAMD involves a complex interplay of genetic risk factors, pro-angiogenic signaling, and chronic inflammation [4]. While several growth factors, including FGF-2 and PDGF, contribute to this process [5], vascular endothelial growth factor (VEGF) is established as the principal driver, promoting endothelial cell proliferation, migration, and vascular permeability [6]. Concur-

rently, innate immune activation, microglia/macrophages recruitment, and the release of inflammatory cytokines such as IL-1β, IL-6, and TNF-α foster a pro-angiogenic microenvironment that sustains and amplifies neovascular growth [7–9]. Collectively, these observations underscore that effective nAMD management likely requires therapeutic strategies that address both angiogenesis and inflammation.

Current first-line therapy for nAMD relies on repeated intravitreal injections of anti-VEGF agents, which have revolutionized patient outcomes by effectively regressing neovascularization and reducing exudation [10,11]. However, significant limitations remain, including incomplete or non-responsiveness in a subset of patients, the development of tachyphylaxis with repeated dosing, a substantial treatment burden, and the cumulative risks of endophthalmitis, geographic atrophy and fibrosis [12,13]. Moreover, conventional anti-VEGF monotherapy does not adequately address the inflammatory component of the disease, highlighting the need for novel agents with broader mechanisms of action [14].

Platelet factor 4 (PF4 or CXCL4), a cationic chemokine abundantly released from activated platelets, is a multifaceted regulator of vascular biology and immune homeostasis [15]. While PF4 is well- established for its potent heparin-neutralizing capacity, which localizes coagulation at injury sites, it also exhibits robust anti-angiogenic activity [16,17]. This function is particularly evident in its inhibition of the VEGF–vascular endothelial growth factor receptor 2 (VEGFR2) signaling axis—the principal driver of angiogenesis [18]. Beyond these vascular functions, emerging evidence underscores PF4's role as an immunomodulator. PF4 has been shown to attenuate neuroinflammation, notably by reducing inflammatory factor expression in the hippocampi of aged mice and in glaucomatous eyes, likely through direct or indirect regulation of microglia/macrophages activity [19,20]. However, its specific expression, functional role, and therapeutic potential in the context of nAMD have remained largely unexplored.

In the current study, we hypothesized that PF4 serves as a regulator capable of concurrently suppressing pathological angiogenesis and mitigating intraocular inflammation—a dual mechanism that could offer a strategic advantage through a more comprehensive therapeutic approach. Accordingly, this study was designed to systematically evaluate the therapeutic efficacy and underlying molecular mechanisms of PF4 in experimental models of nAMD, focusing on its effects on pathological neovascularization, intraocular inflammation, VEGF signaling, and intraocular safety.

2. Materials and Methods

2.1 Animals

Male C57BL/6J mice (6–8 weeks old) were obtained from Beijing Vital River Laboratory Animal Technology (Beijing, China). *Vldlr* knockout (*Vldlr*$^{-/-}$) mice were generated via CRISPR/Cas9-mediated deletion of exons 2–11 of the *Vldlr* 207 transcript. The mice were maintained under a 12-h light/dark cycle in a specific-pathogen-free (SPF) facility at Tianjin Medical University. All procedures were approved by the Institutional Animal Care and Use Committee (IACUC) of Tianjin Medical University (No. TMUaMEC 2024030) and conformed to the ARVO Statement for the Use of Animals in Ophthalmic and Vision Research. For euthanasia, mice were deeply anesthetized with 1.25% tribromoethanol (Avertin; Nanjing Aibei Biotechnology, Nanjing, China) administered intraperitoneally at a dose of 0.2 mL/10 g body weight, followed by cervical dislocation in accordance with the approved ethical guidelines.

2.2 Laser-Induced CNV Model

The laser-induced choroidal neovascularization (CNV) model was established in C57BL/6J mice (6–8 weeks old) as previously described [21]. Briefly, mice were anesthetized, pupils were dilated with 1% tropicamide, and four laser spots (532 nm, 100 mW, 0.15 s, 100 µm spot size) were applied around the optic disc using a 532-nm photocoagulation system (OcuLight GL, Iridex, Mountain View, CA, USA). Formation of a cavitation bubble was taken as confirmation of Bruch's membrane rupture. Eyes with retinal hemorrhage were excluded.

2.3 Intravitreal Injection

For intravitreal injections, the mice were anesthetized with 2%–3% isoflurane in oxygen at a flow rate of 0.5 L/min, and maintained under anesthesia for the duration of the injection procedure (approximately 5-10 min), and pupils were dilated with 1% tropicamide (Sinqi Pharmaceutical, Shenyang, Liaoning, China). A scleral entry site was created with a 30-gauge needle, and a 34-gauge Hamilton syringe was introduced into the vitreous cavity behind the limbus. Mice were randomly assigned to receive 1 µL recombinant human PF4 (0.3 µg/µL in 2% BSA/PBS; R&D Systems, Minneapolis, MN, USA) [22] or vehicle. Topical 0.5% levofloxacin (Sinqi Pharmaceutical, Shenyang, Liaoning, China) was applied before and after injection. Eyes with injection-related hemorrhage or lens injury were excluded from analysis.

2.4 Fundus Fluorescein Angiography (FFA)

FFA was performed at designated time points after laser using a Micron IV retinal imaging system (Phoenix Research Labs, Pleasanton, CA, USA). Mice were anesthetized and pupils dilated with 1% tropicamide. Fluorescein sodium (10%, 100 µL) was injected intraperitoneally, and fundus images were acquired later. Leakage area for each CNV lesion was measured in ImageJ (version 1.53t, National Institutes of Health, Bethesda, MD, USA) by outlining the hyperfluorescent region surrounding the laser

spot as described [21]. The mean leakage area per mouse was calculated for statistical analysis.

2.5 Immunofluorescence of RPE-Choroid Flat-Mounts

For RPE–choroid flat mounts, mice were euthanized and eyes were enucleated and fixed in 4% paraformaldehyde for 1 h. Posterior eyecups were dissected, permeabilized in 1% Triton X-100, and blocked in 3% BSA/0.3% Triton X-100 in PBS. Tissues were incubated with anti-CD31 and anti-Iba1 primary antibodies, followed by fluorophore-conjugated secondary antibodies, and flat-mounted. Z-stack images of each laser lesion were acquired using a confocal microscope (LSM 800; Carl Zeiss, Oberkochen, Germany). CD31-positive neovascular volume and Iba1-positive microglia/macrophages volume were quantified using Imaris software (version 9.0.1, Bitplane AG, Zurich, Switzerland), and the mean value per mouse was used for analysis. The entire procedure was performed essentially as previously described [23]. Sources of antibodies are listed in Table 1.

Table 1. Sources of antibodies used for immunofluorescence.

Antibody	Cat. No.	Company	Dilution Ratio
anti PF4	21157-1-AP	Proteintech	1:200
anti CD31	MAB1398Z	Millipore	1:150
anti Iba1	019-19741	Wako	1:200
anti VEGFA	81323-2-RR	Proteintech	1:200

PF4, platelet factor 4; CD31, cluster of differentiation 31; Iba1, ionized calcium-binding adapter molecule 1; VEGFA, vascular endothelial growth factor A.

2.6 Immunofluorescence of Retinal Sections

For retinal cryosections, eyes were fixed in 4% paraformaldehyde, cryoprotected in 30% sucrose, embedded in Optical Coherence Tomography (OCT) (Sakura Finetek, Torrance, CA, USA), and sectioned at 20 µm. Sections containing laser lesions were permeabilized, blocked in 3% BSA containing 0.3% Triton X-100, and incubated overnight at 4 °C with primary antibodies against CD31, Iba1, vascular endothelial growth factor A (VEGFA), and PF4, followed by the application of fluorophore-conjugated secondary antibodies and DAPI. Sections were imaged by confocal microscopy. Sources of antibodies are listed in Table 1.

2.7 TUNEL Assay

Apoptosis was assessed in retinal sections using a One-step TUNEL (terminal deoxynucleotidyl transferase dUTP nick end labeling) Apoptosis Assay Kit (Cat# C1086, Beyotime Biotechnology, Shanghai, China) according to the manufacturer's instructions. Briefly, cryosections were equilibrated, permeabilized, and incubated with TUNEL reaction mixture, followed by DAPI counterstaining. Images were acquired using a confocal microscope (LSM 800; Carl Zeiss, Oberkochen, Germany).

2.8 Cell Culture

Human retinal microvascular endothelial cells (HRMECs; Procell Life Science & Technology, Wuhan, China) were cultured in endothelial cell medium (ECM; ScienCell Research Laboratories, Carlsbad, CA, USA) supplemented with 5% fetal bovine serum (FBS), 1% endothelial cell growth supplement (ECGS), and 1% penicillin/streptomycin. Cells were maintained at 37 °C in a humidified 5% CO_2 incubator, and passages 3–6 were used for the experiments. The HRMECs were validated by short tandem repeat (STR) profiling and tested negative for mycoplasma contamination by the supplier.

2.9 Cell Viability Assay (CCK-8)

HRMEC viability in response to PF4 and VEGF was assessed using a CCK-8 assay (NCM Biotech, Suzhou, China). Cells were treated with PF4 (0.25, 1, or 4 µg/mL) for 24 h in the presence or absence of VEGF (50 ng/mL). CCK-8 reagent was added for 60 min at 37 °C, and absorbance at 450 nm was measured. Data were normalized to vehicle-treated or VEGF (Sino Biological, Beijing, China) + vehicle controls, as indicated, to identify a non-toxic, effective PF4 concentration for subsequent functional assays.

2.10 Proliferation Assay

HRMEC proliferation was evaluated using a 5-ethynyl-2′-deoxyuridine (EdU) incorporation assay (BeyoClick™ EdU Cell Proliferation Kit; Cat# C0071S, Beyotime Biotechnology, Shanghai, China). Based on CCK-8 assays showing that 1 µg/mL PF4 was the minimum concentration that significantly inhibited VEGF-induced HRMEC proliferation without reducing basal viability, this dose was used in subsequent *in vitro* assays. HRMECs were pretreated with PF4 (1 µg/mL) for 1 h and then stimulated with VEGF (50 ng/mL) for 24 h before EdU labeling and detection.

2.11 Migration Assay

Cell migration was assessed using a scratch wound assay. HRMEC monolayers in 12-well plates were scratched with a 200-µL pipette tip and washed to remove debris. Cells were pretreated with PF4 (1 µg/mL) for 1 h and then stimulated with VEGF (50 ng/mL). Images were acquired at 0 and 12 h, and wound closure was quantified in ImageJ.

2.12 Tube Formation Assay

For tube formation, HRMECs were seeded onto growth factor-reduced Matrigel in 96-well plates. Cells were pretreated with PF4 (1 µg/mL) for 1 h and then exposed to VEGF (50 ng/mL). After 6 h, capillary-like networks were imaged, and total tube length and branch points were quantified using the Angiogenesis Analyzer plugin in ImageJ.

Table 2. Primer sequences used in the experiment.

Gene	Forward	Reverse
Gapdh	TGTGTCCGTCGTGGATCTGA	TTGCTGTTGAAGTCGCAGGAG
Vegfa	GCACATAGAGAGAATGAGCTTCC	CTCCGCTCTGAACAAGGCT
Tnf	CCCTCACACTCAGATCATCTTCT	GCTACGACGTGGGCTACAG
Il1b	CTTTCCCGTGGACCTTCCA	CTCGGAGCCTGTAGTGCAGTT
Il6	TAGTCCTTCCTACCCCAATTTCC	TTGGTCCTTAGCCACTCCTTC
Nfkb1	ATGGCAGACGATGATCCCTAC	CGGAATCGAAATCCCCTCTGTT

Gapdh, glyceraldehyde-3-phosphate dehydrogenase; *Vegfa*, vascular endothelial growth factor A; *Tnf*, tumor necrosis factor; *Il1b*, interleukin-1 beta; *Il6*, interleukin-6; *Nfkb1*, nuclear factor kappa-B subunit 1.

2.13 Enzyme-Linked Immunosorbent Assay (ELISA)

PF4 levels in retina–choroid complexes were determined using a commercial ELISA kit (Cat# ML037257, Shanghai Enzyme-linked Biotechnology, Shanghai, China). Tissues were homogenized in PBS and centrifuged, and supernatants were processed according to the manufacturer's protocol. Absorbance at 450 nm was recorded, and PF4 concentrations were calculated from a standard curve and normalized to total protein.

2.14 Western Blot Analysis

Protein was extracted from HRMECs or retina–choroid complexes using RIPA buffer with protease and phosphatase inhibitors. Protein concentrations were determined by BCA assay. Equal amounts of protein were separated by SDS-PAGE and transferred to PVDF membranes, blocked with 5% non-fat milk, and incubated overnight at 4 °C with primary antibodies against phospho-ERK (Cat# 9101S), total ERK (Cat# 9102S), phospho-AKT (Cat# 2965T), total AKT (Cat# 4691T), phospho-STAT3 (Cat# 4113T), total STAT3 (Cat# 4904T), VEGFR2 (Cat# 9698), (all 1:1000; Cell Signaling Technology, Danvers, MA, USA), β-actin (Cat# 4967L, 1:5000; Cell Signaling Technology, Danvers, MA, USA), and VEGFA (1:1000; Cat# 66828-1-Ig, Proteintech, Wuhan, China). After incubation with HRP-conjugated secondary antibodies, signals were visualized by enhanced chemiluminescence and quantified in ImageJ. All procedures were performed essentially as previously reported [24].

2.15 Quantitative Real-Time PCR

Total RNA from retina–choroid complexes was isolated using a commercial RNA extraction kit (Cat# AC0101, Sparkjade, Jinan, Shandong, China) and reverse-transcribed using Hifair III 1st Strand cDNA Synthesis SuperMix (Cat# 11141ES10, Yeasen, Shanghai, China). qPCR was performed with Hieff® qPCR SYBR Green Master Mix (Low Rox Plus) (Cat# 11202ES60, Yeasen, Shanghai, China) on a LightCycler 480 II system (Roche Diagnostics, Basel, Switzerland). The relative mRNA expression levels of target genes were normalized to the internal control *Gapdh* and quantified using the $2^{-\Delta\Delta Ct}$ method. The primer sequences are listed in Table 2.

2.16 RNA Sequencing and Bioinformatic Analysis

For transcriptomic analysis, retina–choroid complexes were collected from uninjured controls, laser-injured mice receiving vehicle, and laser-injured mice receiving PF4 (n = 3 per group) at day 7 after laser. Tissues were snap-frozen in liquid nitrogen and stored at –80 °C. RNA extraction, library preparation, sequencing, and bioinformatic analysis were performed by Majorbio (Shanghai, China).

2.17 OCT

Spectral-domain OCT (Micron IV, Phoenix Research Labs) was used to assess retinal structure at designated time points after intravitreal injection. Mice were anesthetized and pupils dilated. Circular volume scans centered on the optic disc were obtained, and retinal thickness was measured on ImageJ by masked graders.

2.18 Electroretinography (ERG)

Full-field ERGs were recorded using a Celeris D430 system (Diagnosys, Lowell, MA, USA) as described [25]. Mice were dark-adapted overnight, anesthetized under dim red light, and pupils dilated with tropicamide. Corneal electrodes with integrated stimulators were placed on lubricated corneas, and scotopic responses were elicited at 0.01, 0.1, and 1 cd·s/m^2. a- and b-wave amplitudes were analyzed.

2.19 Retinal Toxicity Evaluation

To evaluate the potential retinal toxicity of PF4, C57BL/6J mice received a single intravitreal injection of PF4 (0.3 µg in 1 µL) or vehicle (PBS) on day 0. At day 7 post-injection, the mice were subjected to a series of safety assessments. First, fundus imaging and OCT were performed to examine the gross morphology and retinal thickness. Subsequently, retinal function was assessed using ERG as described in the previous section. Following functional testing, the mice were euthanized, and the eyes were harvested for histological analysis, including hematoxylin and eosin (H&E) staining to evaluate structural integrity and a TUNEL assay to detect cell apoptosis.

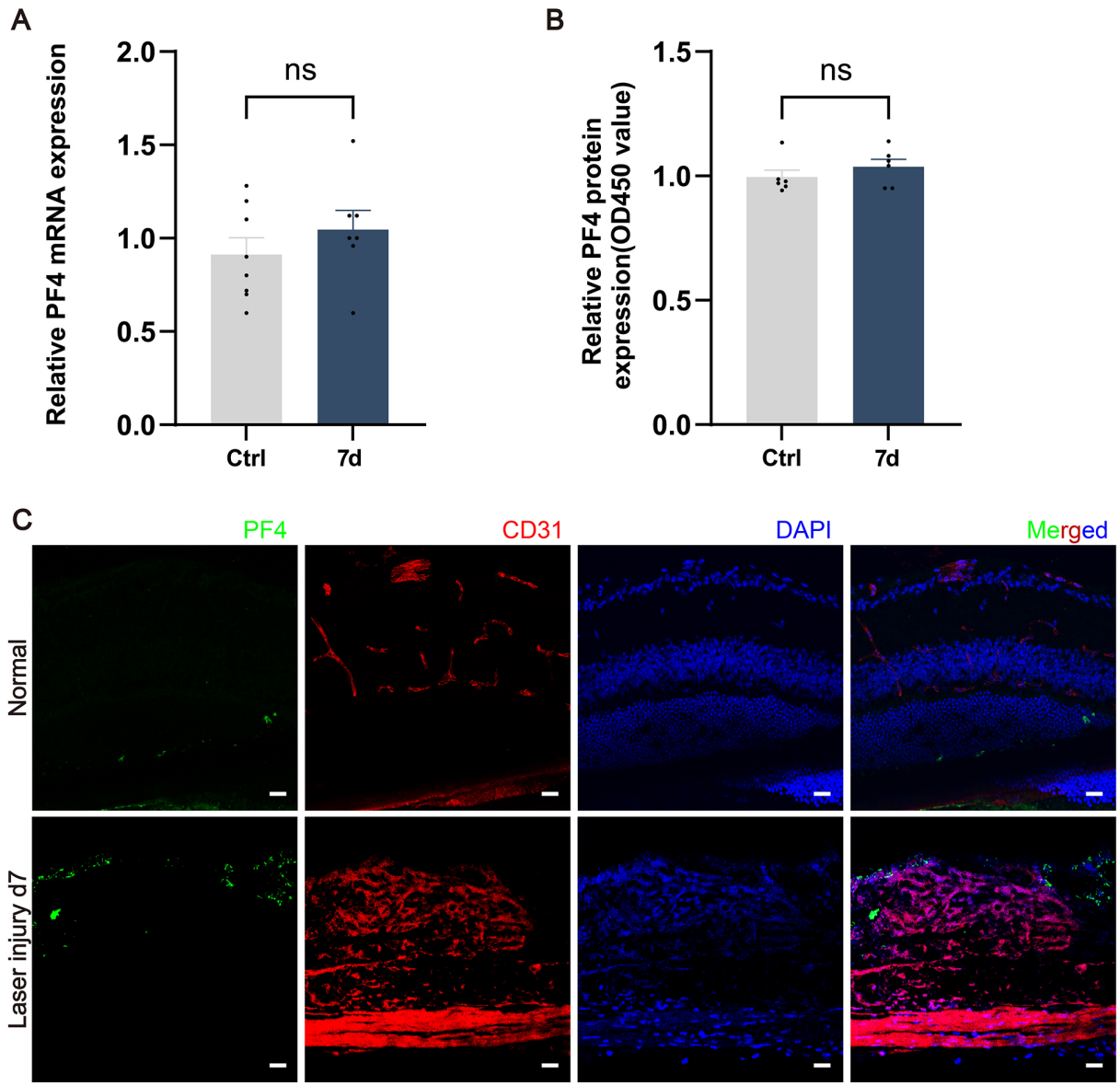

Fig. 1. PF4 expression after laser application. (A) *Pf4* mRNA levels in the laser lesions of adult mice (6–8 weeks old) at the indicated time points after laser injury, measured by quantitative real-time PCR (qRT-PCR). n = 7 eyes (from 4 mice) per group. (B) PF4 protein levels, measured by ELISA. n = 4 eyes (from 3 mice) per group. (C) Representative immunofluorescence images of PF4 (green) and CD31 (red) in cross-sections of the retinas from Normal control and laser-induced CNV mice at day 7 post-injury; nuclei are counterstained with DAPI (blue). Scale bar = 20 µm. Data are shown as mean ± SEM. ns $p \geq 0.05$. Two-tailed Student's *t*-test was used for comparison between two groups (A and B). PF4, platelet factor 4; ELISA, enzyme-linked immunosorbent assay; CNV, choroidal neovascularization; DAPI, 4',6-diamidino-2-phenylindole; SEM, standard error of the mean.

2.20 Statistical Analysis

Data were analyzed using GraphPad Prism version 10 (GraphPad Software, San Diego, CA, USA). All results are expressed as mean ± standard error of the mean (SEM). For comparisons between two groups, an unpaired two-tailed Student's *t*-test was performed. For comparisons among multiple groups, one-way analysis of variance (ANOVA) followed by Tukey's post hoc test was used. A *p* value of less than 0.05 was considered statistically significant.

3. Results

3.1 PF4 Expression in Laser-Induced CNV

To define PF4 expression in mouse CNV, we measured PF4 expression in a laser-induced CNV mouse model (Fig. 1A–C). Quantitative real-time PCR (qRT-PCR) showed that *Pf4* mRNA levels were not significantly changed at day 7 after laser injury in posterior segment tissues compared with Normal control (i.e., untreated healthy mice) (Fig. 1A). Consistently, ELISA detected no significant difference in PF4 protein levels in posterior eye lysates

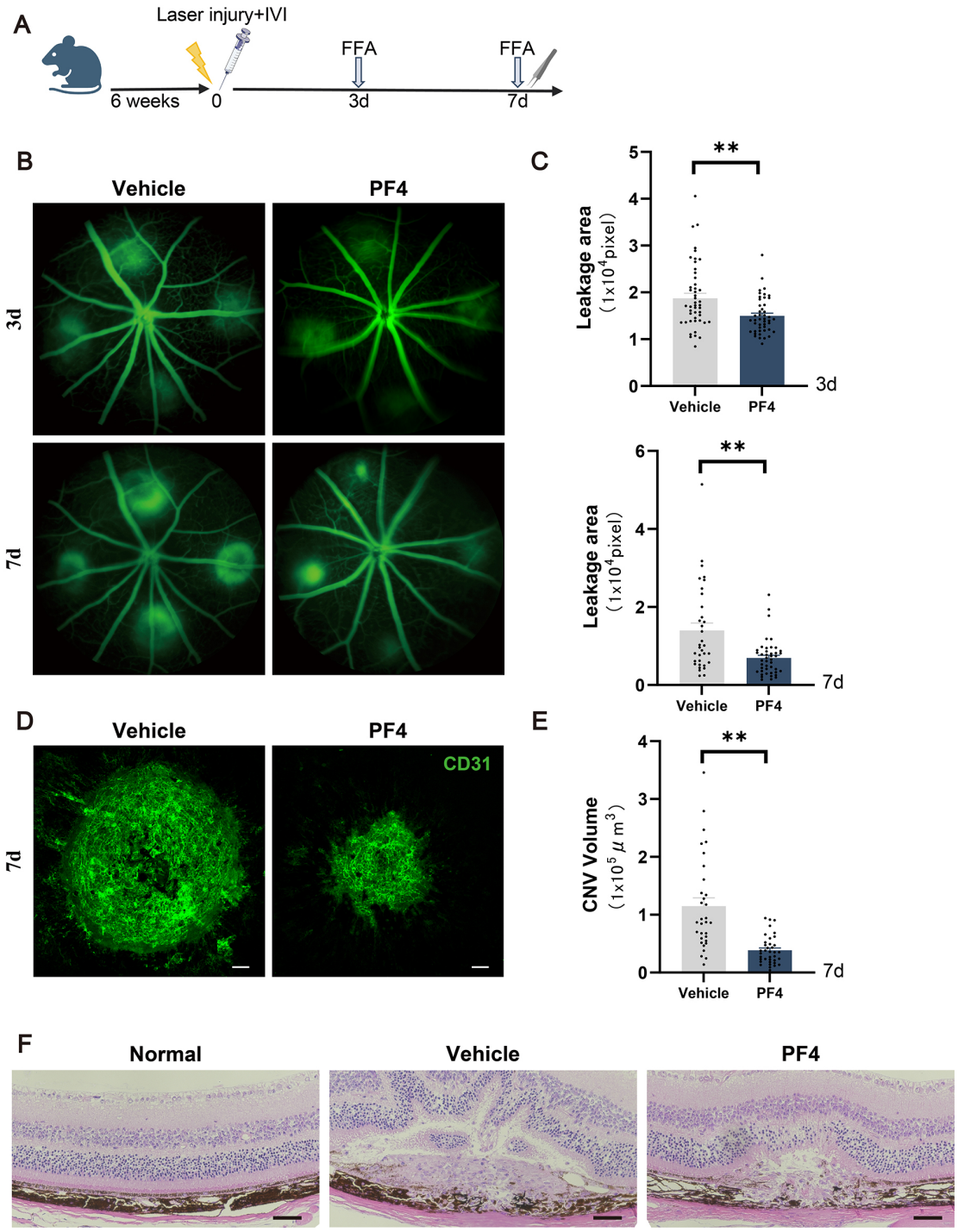

Fig. 2. PF4 administration attenuates vascular leakage and choroidal neovascularization in a laser-induced mouse model of CNV. (A) Schematic of the laser injury, intravitreal injection, and analysis schedule. (B) Representative longitudinal paired FFA images showing vascular leakage in the same eyes at days 3 and 7 after laser injury in vehicle- and PF4-treated mice. (C) Quantification of leakage area at days 3 and 7 is shown in (B). n = 30 lesions from 5 mice per group. (D) Representative confocal images of RPE–choroid flat mounts at day 7 after laser injury from vehicle- and PF4-treated mice, stained for CD31 (green) to visualize CNV lesions. Scale bar = 50 µm. (E) Quantification of CNV volume shown in (D), assessed as CD31-positive fluorescence volume. n = 32 lesions from 5 mice per group. (F) Representative retinal sections stained with H&E from Normal, vehicle-treated, and PF4-treated mice. Scale bar = 50 µm. Data are shown as mean ± SEM. $^{**}p < 0.01$. Two-tailed Student's *t*-test was used for comparison between two groups. FFA, fundus fluorescein angiography; RPE, retinal pigment epithelium; H&E, hematoxylin and eosin. Fig. 2A was created using Adobe Illustrator 2025.

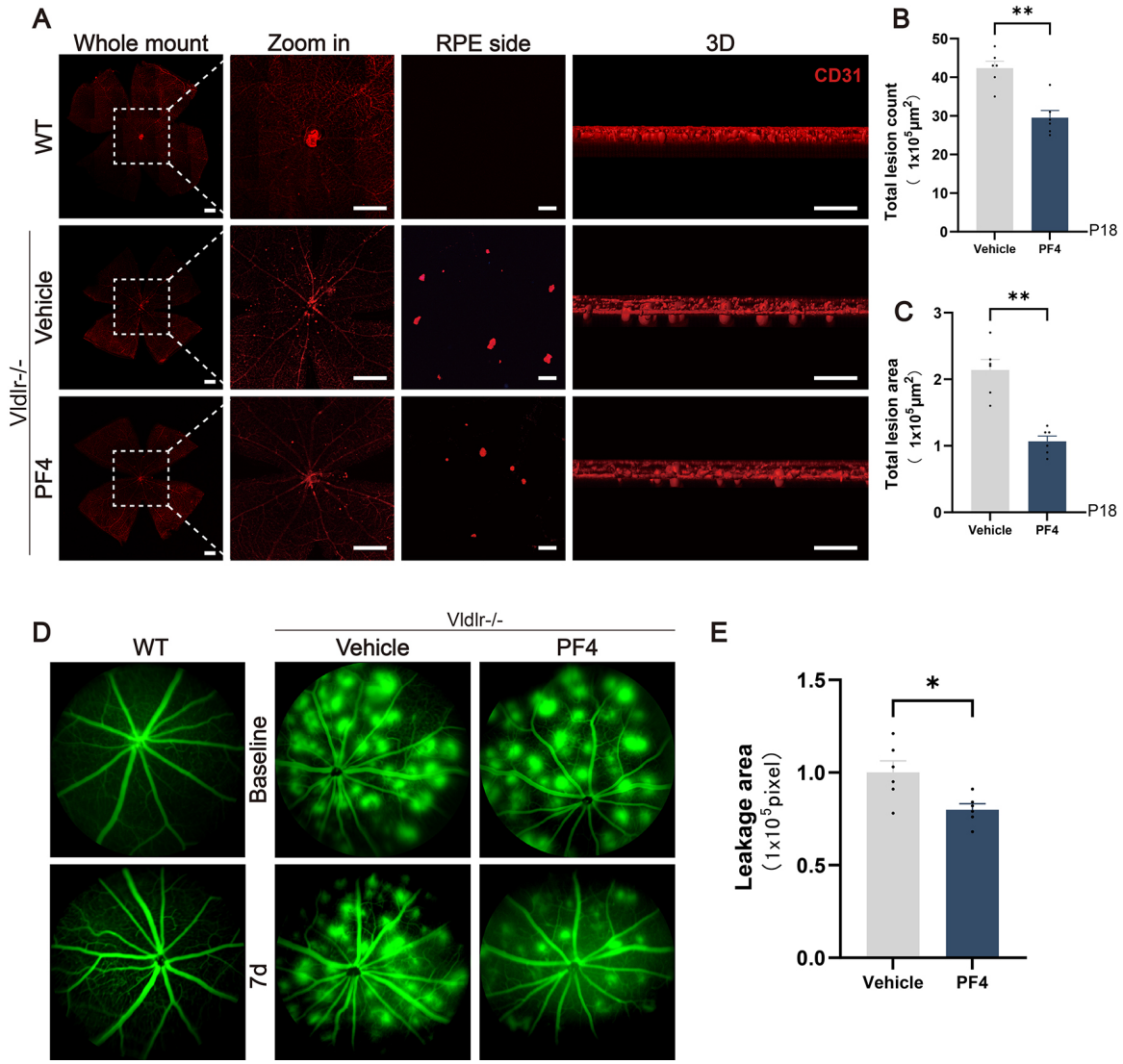

Fig. 3. PF4 administration attenuates vascular leakage retinal neovascularization in Vldlr$^{-/-}$ mice. (A) Representative confocal images of retinal flat mounts from wild-type (WT), vehicle-treated Vldlr$^{-/-}$, and PF4-treated Vldlr$^{-/-}$ mice following CD31 (red) immunostaining. Whole-mount views, magnified regions (zoomed in), images from the RPE side, and corresponding three-dimensional (3D) reconstructions illustrating abnormal vascular growth are shown. Scale bar = 500 µm (whole mount), 167 µm (zoomed in), 50 µm (RPE side), and 50 µm (3D). (B,C) Quantifications of the lesion number and lesion area are shown in (A). n = 6 eyes (from 3 mice) per group. (D) Adult Vldlr$^{-/-}$ mice received intravitreal injections of the indicated treatments (Vehicle or PF4) and were analyzed on day 7. Representative FFA images show vascular leakage at baseline (day 0, pre-injection) and at day 7 post-injection in Vehicle-treated Vldlr$^{-/-}$ and PF4-treated Vldlr$^{-/-}$ mice, compared with age-matched healthy WT controls. (The two WT images are biological replicates from independent mice, demonstrating the consistent absence of vascular leakage in healthy retinas.) (E) Quantification of leakage area post-treatment is shown in (D). n = 6 eyes (from 3 mice) per group. Data are shown as mean ± SEM. *$p < 0.05$, **$p < 0.01$. Two-tailed Student's *t*-test was used for comparison between two groups. Vldlr$^{-/-}$, very low-density lipoprotein receptor knockout.

at day 7 post-laser (Fig. 1B). Immunofluorescence further revealed only weak PF4 signals in both Normal and laser-injured eyes, without an apparent increase within laser lesions (Fig. 1C).

3.2 PF4 Inhibits Pathological Neovascularization in Multiple Mouse Models

To investigate the role of PF4 in pathological neovascularization, we initially utilized a laser-induced mouse model of CNV. Six-week-old mice underwent laser induction, followed by intravitreal injection of PF4 protein (Fig. 2A). We first assessed the hallmark feature of CNV,

vascular leakage, by FFA on day 3 post-laser. FFA images demonstrated that dye leakage was markedly reduced in PF4-treated mice at days 3 and 7 after laser injury (Fig. 2B). Quantitative analysis further confirmed this robust inhibitory effect, showing a significant reduction in leakage area in the PF4-treated group at both time points (Fig. 2C). We then evaluated the extent of neovascularization by performing CD31 immunofluorescence staining on RPE–choroid flat mounts at day 7 post-laser. Representative confocal images revealed that CNV lesions were noticeably smaller in PF4-treated mice than in Vehicle (i.e., mice injected with the carrier solution without PF4) (Fig. 2D). Quantification of CNV volume corroborated these findings, demonstrating a significant decrease in lesion volume in the PF4-treated group (Fig. 2E). To validate these results histologically, we performed H&E staining on retinal cross-sections. H&E images showed a clear reduction of CNV lesions in PF4-treated eyes (Fig. 2F).

To further evaluate the protective role of PF4, we employed the Vldlr$^{-/-}$ mouse model, which recapitulates key features of human neovascular retinal diseases [26]. Vldlr$^{-/-}$ mice develop pathological retinal neovascularization (PRNV) from postnatal day 11 (P11), accompanied by progressive retinal ischemia, breakdown of the outer blood–retinal barrier, and functional decline. This pathology stems from impaired RPE lipid transport, resulting in HIF-driven upregulation of proangiogenic factors such as VEGF, mirroring the pathogenesis of proliferative diabetic retinopathy and nAMD [27].

We intravitreally injected PF4 or vehicle into Vldlr$^{-/-}$ mice at P11 and analyzed retinal angiogenesis at P18. CD31 immunostaining of retinal flat mounts revealed marked reduction in neovascular lesions in PF4-treated eyes compared with Vehicle, with higher-magnification and three-dimensional (3D)-reconstructed images further demonstrating attenuated aberrant vascular growth (Fig. 3A). Quantitative analysis confirmed that PF4 significantly decreased both the number and area of neovascular lesions (Fig. 3B,C). Similarly, in adult Vldlr$^{-/-}$ mice, PF4 injection reduced vascular leakage, as evaluated by FFA at baseline (i.e., the pre-injection time point, day 0) and 7 days post-injection (Fig. 3D). Quantification showed a significant improvement in vascular leakage following PF4 treatment (Fig. 3E).

3.3 PF4 Suppresses Intraocular Inflammation Induced by Laser Injury

Because inflammation contributes to CNV, we examined whether PF4 modulates laser-induced inflammatory responses. Compared with vehicle, PF4 significantly reduced mRNA levels of Il1b, Il6, Tnf, and Nfkb1 in posterior segment retinal tissues at day 7 post-laser injury (Fig. 4A). We next assessed microglia/macrophages recruitment at lesion sites. Immunostaining showed fewer Iba1^{+} microglia/macrophages with reduced aggregation in PF4-treated eyes (Fig. 4B), and quantitative analysis confirmed reduced Iba1^{+} microglia/macrophages volume within lesions (Fig. 4C).

To comprehensively characterize PF4-mediated transcriptomic changes, we performed bulk RNA sequencing of retina–choroid complexes from Normal, vehicle-treated, and PF4-treated mice. Hierarchical clustering of differentially expressed genes (DEGs) across the three groups revealed clearly segregated expression profiles (Fig. 4D). Vehicle-treated samples displayed a pronounced proinflammatory signature, whereas PF4-treated samples formed a distinct cluster whose expression pattern partially shifted toward that of Normal controls, suggesting that PF4 counteracts injury-induced inflammatory reprogramming. Differential expression analysis between the Vehicle and PF4 groups showed that PF4 induced widespread transcriptional remodeling (Fig. 4E). PF4 significantly downregulated a broad set of inflammation-related genes, including chemokines, cytokines, adhesion molecules, and genes associated with leukocyte trafficking and microglia/macrophages activation, while genes involved in tissue homeostasis were relatively preserved. We interrogated the biological processes associated with PF4-regulated genes using GO enrichment analysis. PF4-downregulated DEGs were predominantly enriched in terms related to innate immune responses, cytokine production, regulation of inflammatory responses, and responses to external stimuli (Fig. 4F), indicating broad suppression of inflammatory activation programs. We then examined pathway changes using KEGG enrichment analysis, which revealed that PF4 strongly inhibited signaling cascades implicated in retinal inflammation and leukocyte recruitment, including the NF-κB and JAK–STAT signaling pathways, chemokine signaling, cell adhesion molecule pathways, leukocyte transendothelial migration, and immune-related pathways (Fig. 4G).

3.4 PF4 Downregulates VEGF Expression in CNV Lesions

Given that inflammatory mediators can induce VEGFA expression [28–33], we tested whether PF4 affects VEGFA levels in laser-induced CNV. Compared with the Normal control group, laser photocoagulation markedly increased VEGFA protein expression in the RPE–choroid complex, whereas PF4 treatment significantly attenuated this upregulation (Fig. 5A,B). Consistent with the western blot results, immunofluorescence staining of sections through the laser lesions revealed strong immunoreactivity of VEGFA around CD31-positive neovessels in the vehicle group, which was markedly reduced in PF4-treated eyes (Fig. 5C). These findings suggest that PF4 may inhibit CNV formation at least in part by suppressing inflammation-driven upregulation of VEGFA.

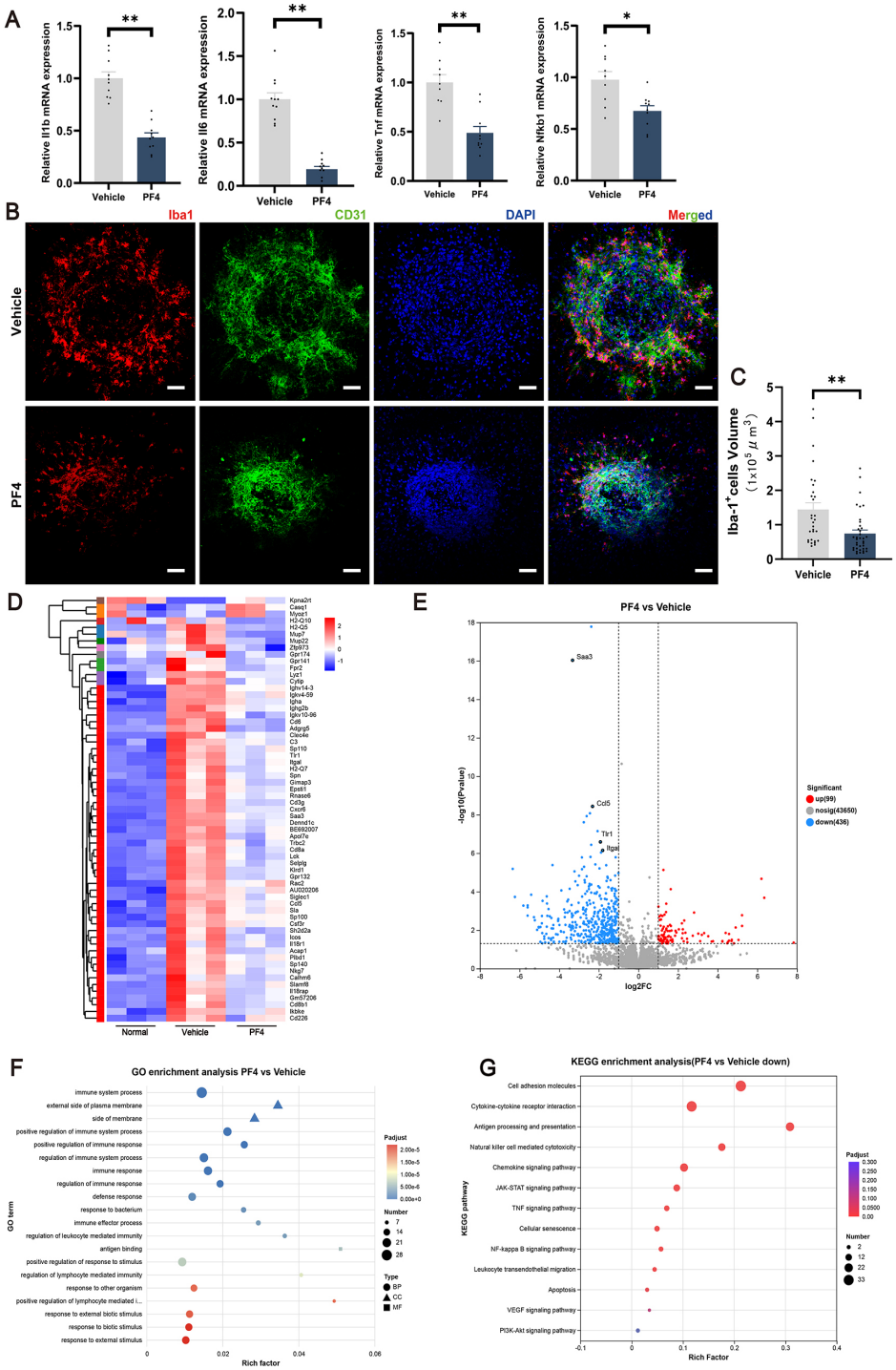

Fig. 4. PF4 suppresses intraocular inflammation induced by laser injury. (A) Relative mRNA expression of Il1b, Il6, Tnf, and Nfkb1 in the posterior segment 7 days after laser photocoagulation in vehicle- and PF4-treated eyes. (B) Representative confocal images of laser lesions from vehicle- and PF4-treated retinas immunostained for Iba1 (red) and CD31 (green), with nuclei counterstained with DAPI (blue). Scale bar = 50 μm. (C) Quantification of Iba1$^+$ microglia/macrophages volume within the laser lesions shown in (B). n = 32 lesions (from 5 eyes) per group. (D) Heatmap of differentially expressed genes in retina–choroid complexes from Normal, vehicle-treated, and PF4-treated mice. (E) Volcano plot of differentially expressed genes in PF4-treated versus vehicle-treated groups. (F) GO enrichment analysis of differentially expressed genes between PF4- and vehicle-treated groups. (G) KEGG pathway enrichment analysis of differentially expressed genes between PF4- and vehicle-treated groups. n = 3 eyes (from 3 mice) per group for RNA sequencing. Data are shown as mean ± SEM. *$p < 0.05$, **$p < 0.01$. Two-tailed Student's *t*-test was used for comparison between two groups. Il1b, interleukin-1 beta; Il6, interleukin-6; Tnf, tumor necrosis factor; Nfkb1, nuclear factor kappa-B subunit 1; GO, Gene Ontology; KEGG, Kyoto Encyclopedia of Genes and Genomes.

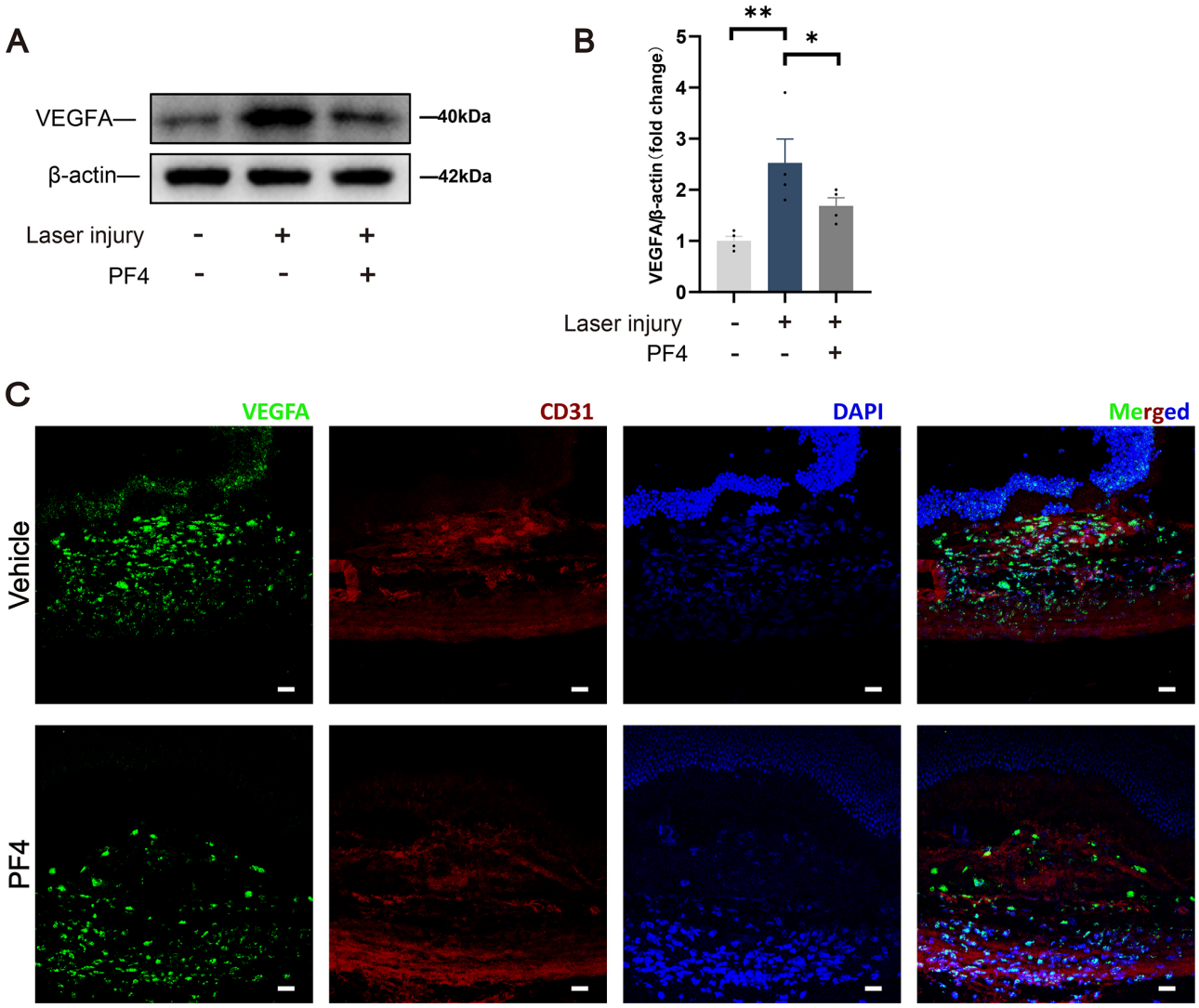

Fig. 5. PF4 attenuates VEGFA expression in laser-induced CNV lesions. (A) Representative immunoblot of VEGFA expression in Normal (no laser), laser-injured + vehicle, and laser-injured + PF4–treated eyes. β-Actin served as a loading control. (B) Quantification of VEGFA protein levels normalized to β-actin and expressed as fold change relative to the sham group. n = 4 eyes (from 4 mice) per group. (C) Representative confocal images of posterior segment from laser-injured eyes treated with vehicle or PF4, showing VEGFA (green), CD31-positive vascular endothelium (red), and nuclei (DAPI, blue), scale bar = 20 µm. Data are shown as mean ± SEM. *$p <$ 0.05, **$p < 0.01$. One-way ANOVA was used for the comparison of multiple groups. ANOVA, analysis of variance.

3.5 PF4 Inhibits VEGF-Induced Angiogenesis In Vitro

In addition to suppressing inflammation-driven upregulation of VEGFA *in vivo*, we sought to investigate whether PF4 could counteract VEGF-induced angiogenic responses in endothelial cells *in vitro*. We initially investigated the impact of this factor on key angiogenic processes *in vitro* using HRMECs—a type of vascular endothelial cell that highly expresses VEGFR2 and is highly sensitive to VEGF stimulation [34–37].

The results showed that the number of proliferating HRMECs was markedly reduced in the PF4-pretreated group compared with the group stimulated with VEGF alone (Fig. 6A). Quantitative analysis further revealed a significant decrease in the percentage of EdU-positive cells (Fig. 6B). We next assessed cell migration capacity using a scratch wound-healing assay, which revealed that PF4 pretreatment significantly suppressed VEGF-stimulated migration of HRMECs (Fig. 6C). The scratch closure rate was significantly lower in the PF4-treated group than in the control group (Fig. 6D). Furthermore, we examined the effect of PF4 on the ability of HRMECs to form capillary-like tubular structures, a critical step in the angiogenesis process. The results demonstrated that PF4 pretreatment disrupted VEGF-driven tube formation in HRMECs (Fig. 6E). The number of branch points was reduced in the PF4-treated group compared with the VEGF control group (Fig. 6F).

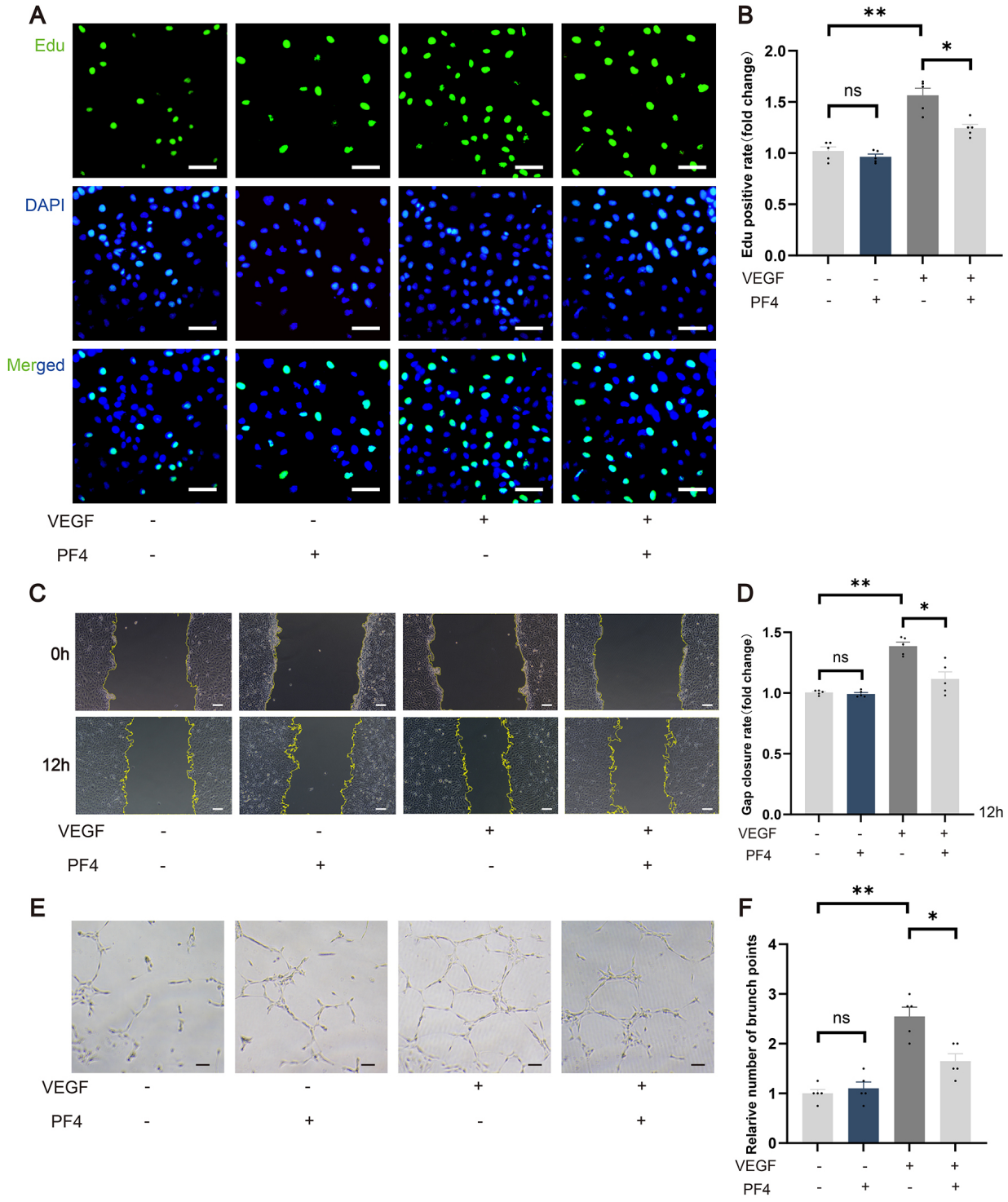

Fig. 6. PF4 inhibits VEGF-induced proliferation, migration, and tube formation of human retinal microvascular endothelial cells. (A) Representative EdU staining of HRMECs after PF4 pretreatment and VEGF stimulation, stained for EdU (green) and DAPI (blue). Scale bar = 50 µm. (B) Quantification of EdU-positive cells as a percentage of total cells in (A). n = 5 per group. (C) Representative images of HRMEC migration in a scratch-wound assay at 0 and 12 hours after PF4 pretreatment and VEGF stimulation. Scale bar = 50 µm. (D) Quantification of gap closure in (C). n = 5 per group. (E) Representative images of tube formation by HRMECs following PF4 pretreatment and VEGF stimulation. Scale bar = 100 µm. (F) Quantification of branch points in (E). n = 5 per group. Data are shown as mean ± SEM. *$p < 0.05$, **$p < 0.01$, ns $p \geq 0.05$. One-way ANOVA was used for the comparison of multiple groups. VEGF, vascular endothelial growth factor; HRMECs, human retinal microvascular endothelial cells.

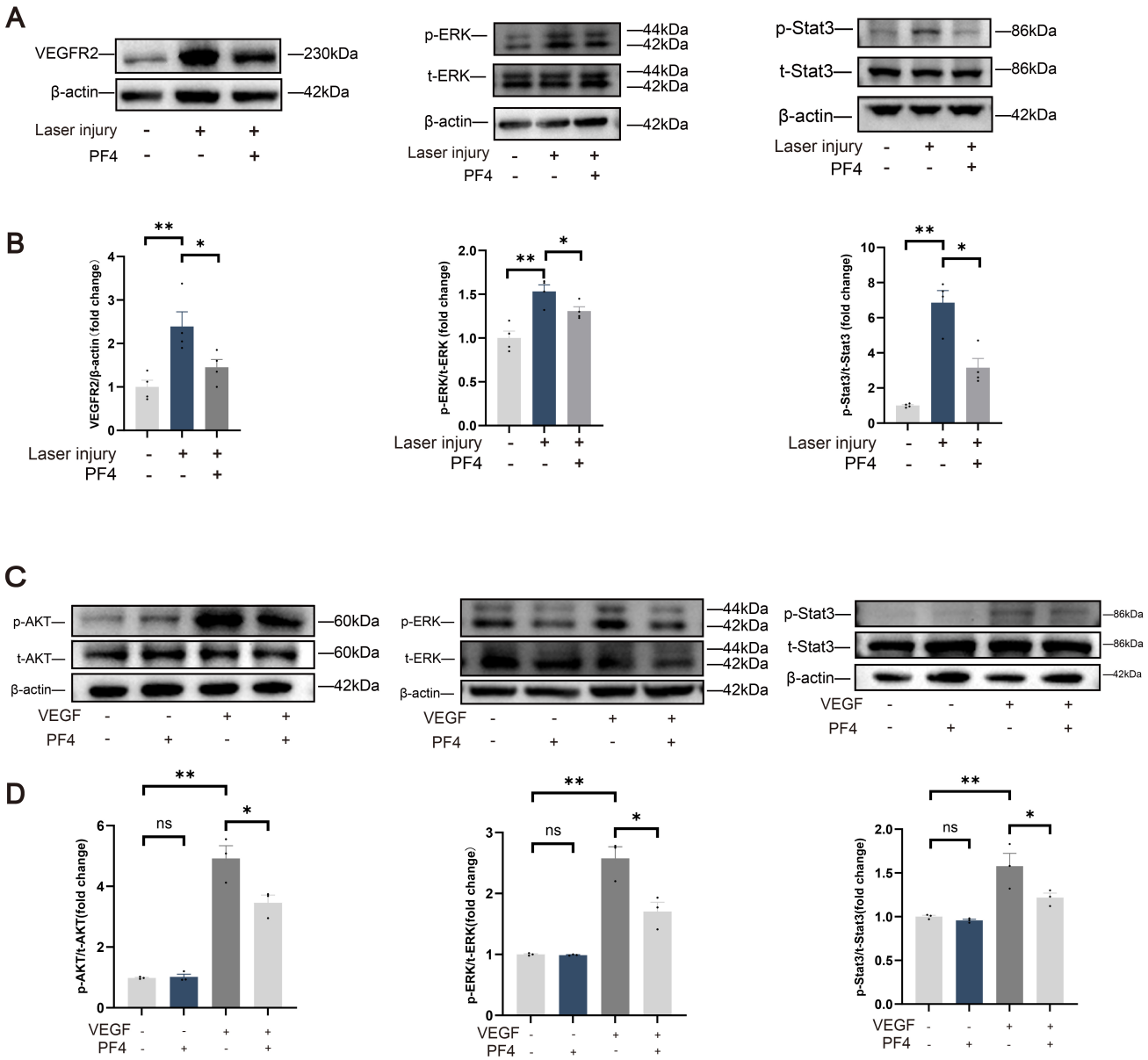

Fig. 7. PF4 attenuates VEGF/VEGFR2-driven ERK, AKT, and STAT3 signaling *in vivo* and *in vitro*. (A) Representative immunoblots of VEGFR2, phosphorylated (p-ERK) and total (t-ERK) ERK, and phosphorylated (p-STAT3) and total (t-STAT3) STAT3 in RPE–choroid–sclera complex tissue from sham (no laser), laser-injured + vehicle, and laser-injured + PF4–treated mice. β-Actin served as a loading control. (B) Densitometric analysis of VEGFR2/β-actin, p-ERK/t-ERK, and p-STAT3/t-STAT3 expression in (A), shown as fold change relative to control. n = 4 eyes (from 4 mice) per group. (C) Representative immunoblots of phosphorylated and total AKT (p-AKT, t-AKT), ERK, and STAT3 in HRMECs stimulated with VEGF in the presence or absence of PF4. (D) Quantification of p-AKT/t-AKT, p-ERK/t-ERK, and p-STAT3/t-STAT3 in (C), expressed as fold change relative to unstimulated cells. n = 3 per group. Data are shown as mean $\pm$ SEM. *$p < 0.05$, **$p < 0.01$, ns $p > 0.05$. One-way ANOVA was used for the comparison of multiple groups. VEGFR2, vascular endothelial growth factor receptor 2; ERK, extracellular signal-regulated kinase; AKT, protein kinase B; STAT3, signal transducer and activator of transcription 3.

3.6 PF4 Attenuates VEGF-Driven VEGF-R2, ERK/AKT/STAT3 Signaling In Vivo and In Vitro

To elucidate the molecular basis underlying these anti-angiogenic effects of PF4, we next examined whether PF4 modulates VEGF/VEGFR2 signaling and its key downstream pathways [38,39]. In the laser-induced CNV mouse model, PF4 administration markedly reduced VEGFR2 expression, as well as the phosphorylation of ERK and STAT3 in choroidal tissue (Fig. 7A,B), indicating that PF4 attenuates VEGF/VEGFR2-related signal transduction *in vivo*. Consistent with these findings, PF4 significantly inhibited VEGF-induced phosphorylation of AKT, ERK, and STAT3

in cultured HRMECs (Fig. 7C,D), further supporting its direct suppression of VEGF/VEGFR2-driven pro-angiogenic signaling.

3.7 Intravitreal PF4 Administration Exhibits a High Retinal Safety Profile

We next evaluated the retinal safety of intraocular PF4 administration in mice at day 7 post-injection. OCT imaging showed that retinal morphology and thickness were preserved following intraocular injection of either vehicle or PF4 (Fig. 8A,B). Consistently, ERG revealed no significant reduction in a-wave amplitudes (originating primarily from photoreceptor rods and cones) or b-wave amplitudes (reflecting inner retinal activity, mainly Müller and bipolar cells) in PF4-treated eyes compared with vehicle-treated controls (Fig. 8C,D). Histological examination further confirmed the structural integrity of the retina (Fig. 8E), and TUNEL staining demonstrated an absence of appreciable cell death (Fig. 8F). Taken together, these data indicate that a single intraocular administration of PF4 (0.3 µg/eye) was well tolerated and exhibited a favorable retinal safety profile in mice.

4. Discussion

In this study, we evaluated the therapeutic potential of PF4 in experimental animal models of nAMD. Our results demonstrated that intravitreal PF4 injection significantly reduced vascular leakage and CNV lesion size in the laser-induced mouse CNV model. These findings were further supported by results obtained in Vldlr$^{-/-}$ mice, in which retinal neovascularization was suppressed. In parallel with the *in vivo* studies, we showed that PF4 inhibited VEGF-induced proliferation, migration, and tube formation in HRMECs, indicating a consistent anti-angiogenic effect across experimental systems.

A key finding from our work is the absence of significant upregulation of endogenous *Pf4* mRNA or protein in laser-induced CNV lesions at the time point the specimens were collected (Fig. 1A–C), which provides critical context for subsequent experiments. Despite PF4's established anti-angiogenic and immunomodulatory properties in systemic models [38,39] (e.g., tumor angiogenesis, atherosclerosis), the lack of a reported response to laser injury in the retina suggests a "therapeutic gap" in the ocular inflammatory-angiogenic cascade. This observation justifies the use of exogenous PF4 supplementation, as endogenous levels are insufficient to counteract pathological neovascularization or inflammation. Notably, weak PF4 immunoreactivity in injured eyes (Fig. 1C) further supports the need for targeted delivery.

Building on this rationale, we validated PF4's anti-angiogenic efficacy across two distinct mouse models of neovascular retinal disease: laser-induced CNV (mimicking nAMD) and Vldlr$^{-/-}$ mice (recapitulating retinal ischemia and PRNV, as seen in retinopathy of prematurity or diabetic retinopathy) [40,41]. In the laser-induced CNV model, PF4 significantly reduced vascular leakage (FFA; Fig. 2B,C) and CNV lesions, as shown by CD31 and H&E staining (Fig. 2D–F), demonstrating attenuation of both functional and structural hallmarks of pathological angiogenesis. In Vldlr$^{-/-}$ mice, PF4 similarly reduced neovascular lesion number and area (P18; Fig. 3A–C) and vascular leakage (adult mice; Fig. 3D,E). Although the Vldlr$^{-/-}$ model is primarily driven by metabolic fuel shortages, its pathological progression involves secondary inflammatory cell infiltration. The consistent efficacy of PF4 across both laser-induced (acute/inflammatory) and Vldlr$^{-/-}$ (chronic/metabolic) models suggests potential utility across diverse pathological contexts [42]. These cross-model results are particularly impactful, as they confirm PF4's efficacy in the inhibition of retinal angiogenesis regardless of the initial trigger (laser-induced choroidal ischemia vs. developmental retinal ischemia in Vldlr$^{-/-}$ mice). This versatility suggests that PF4 may act on pathways common to pathological angiogenesis, warranting further investigation across multiple neovascular retinal diseases. Importantly, the concordance between functional (FFA) and structural (immunostaining and H&E) outcomes strengthens the conclusion that PF4 suppresses neovessel formation and vascular leakage, rather than merely masking functional deficits.

Our results demonstrate that PF4 suppresses laser-induced inflammation at both molecular and cellular levels: (1) reduced mRNA expression of proinflammatory mediators (Il1b, Il6, Tnf, and Nfkb1; Fig. 4A); (2) decreased recruitment of activated Iba1^{+} microglia/macrophages to lesion sites (Fig. 4B,C); and (3) broad transcriptional remodeling of inflammation-related pathways (RNA-seq; Fig. 4D–G). Bulk RNA-seq analysis further reveals that PF4 inhibits injury-induced inflammatory reprogramming: PF4-treated samples cluster closer to uninjured controls (Fig. 4D) and downregulate genes involved in innate immunity, cytokine production, and leukocyte trafficking (GO enrichment; Fig. 4F). KEGG pathway analysis identifies key suppressed signaling cascades, including NF-κB, JAK–STAT, VEGF, PI3/AKT, and chemokine signaling (Fig. 4G)—pathways known to promote both inflammation and angiogenesis in the retina. These findings indicate that PF4's anti-angiogenic effects are partially mediated by its anti-inflammatory properties, addressing a critical "upstream" driver of PRNV. The reduction in microglia/macrophage activation is particularly notable, as activated microglia/macrophages are producers of VEGF and proinflammatory cytokines in CNV lesions, making them a key therapeutic target. Clinical studies have shown that combining anti-VEGF with anti-inflammatory therapy can improve outcomes in nAMD [43,44], supporting the potential translational relevance of PF4's dual mechanism.

Given the central role of VEGF in ocular neovascularization, we further investigated whether PF4 targets VEGF-driven pathways, uncovering a dual mechanism of action.

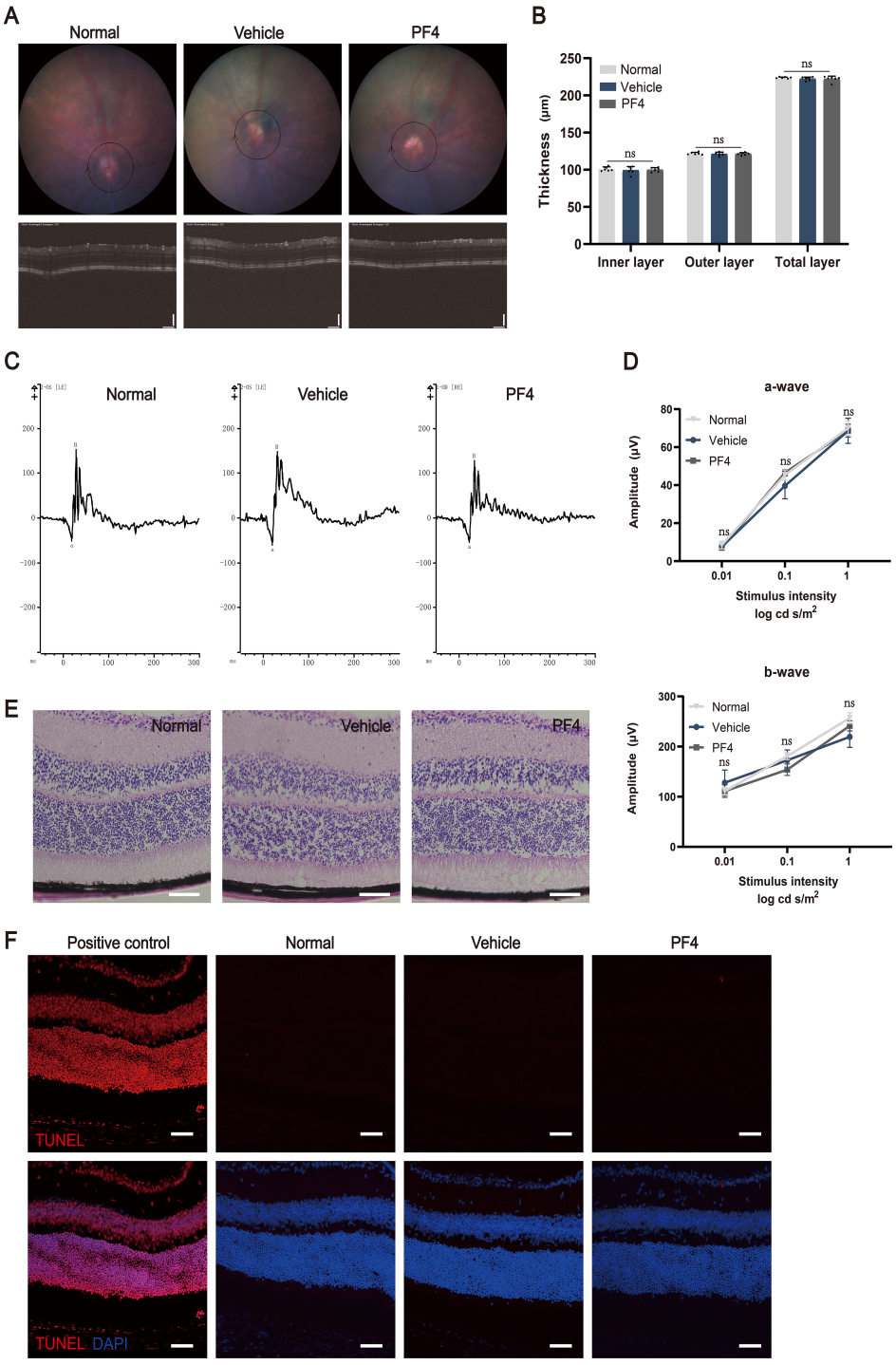

Fig. 8. Evaluation of retinal toxicity following the intravitreal administration of PF4 in mice. (A) Representative fundus imaging and OCT imaging of normal mice and mice treated with vehicle or PF4. The circular bounding box in the OCT images indicates the standardized region scanned and used for layer thickness measurement. (B) Thickness of total retinal layers. n = 6 eyes (from 3 mice) per group. (C) Representative electroretinogram imaging of normal mice and mice treated with vehicle or PF4, where "a" and "B" denote the a-wave and b-wave amplitudes, respectively. The y-axis represents response amplitude in microvolts (μV). (D) Electroretinogram and quantification of normal mice and mice treated with vehicle or PF4. n = 6 eyes (from 3 mice) per group. (E) H&E staining of eyeball sections from normal mice and mice treated with vehicle or PF4. Scale bar = 100 μm. (F) TUNEL assay of retinal sections from normal mice and mice treated with vehicle or PF4. Scale bar = 50 μm. Data are shown as mean ± SEM. ns $p \geq 0.05$. One-way ANOVA was used for the comparison of multiple groups. OCT, Optical Coherence Tomography; TUNEL, terminal deoxynucleotidyl transferase dUTP nick end labeling.

In laser-induced CNV, PF4 significantly attenuated laser-induced VEGF upregulation (western blot and immunofluorescence; Fig. 5A–C), likely via suppression of inflammation (since IL-1β, IL-6, and NF-κB are known VEGF inducers). Beyond reducing VEGF expression, PF4 directly inhibits VEGF-mediated angiogenic responses *in vitro*: pretreatment of HRMECs (vascular endothelial cells highly sensitive to VEGF) with PF4 suppressed VEGF-induced proliferation (EdU assay; Fig. 6A,B), migration (scratch assay; Fig. 6C,D), and tube formation (Fig. 6E,F)—three critical steps in angiogenesis. Mechanistically, PF4 attenuates canonical VEGF downstream signaling: *in vivo* (laser-induced CNV), PF4 reduced VEGFR2 expression and phosphorylation of ERK and STAT3 (Fig. 7A,B); *in vitro* (HRMECs), PF4 suppressed the phosphorylation of ERK, AKT, and STAT3 (Fig. 7C,D). Regarding the biochemical interaction with the VEGF axis, the observed suppression by PF4 likely involves a tripartite inhibitory mechanism: direct sequestration, competitive interference, and receptor-mediated signaling antagonism. First, the highly cationic surface of PF4 enables it to physically sequester the anionic heparin-binding domain of VEGF-A, forming inactive complexes that effectively reduce its bioavailability [45]. Second, PF4 exerts competitive interference by occupying heparan sulfate (HS) proteoglycan binding sites on the endothelial cell surface; since these HS sites are essential co-receptors for stabilizing the VEGF–VEGFR2 interaction, their blockage significantly impairs receptor activation [45]. Finally, beyond ligand-level interference, PF4 directly targets endothelial cells via its cognate receptor, CXCR3-B, triggering downstream anti-proliferative signaling that functionally counteracts the VEGF-induced angiogenic cascade [46]. This multi-layered antagonism—neutralizing the ligand, blocking co-receptor access, and activating inhibitory receptors—explains the robust suppression of angiogenesis observed in our study [46]. Together, these data support a dual mechanism for PF4: (1) indirect inhibition via suppression of inflammation-driven VEGF upregulation; and (2) direct inhibition of VEGF-induced signaling and endothelial cell function. This dual action may offer therapeutic benefits that complement those of single-target agents such as anti-VEGF antibodies, though direct comparative studies are needed. For clinical applicability, ocular safety is paramount—intravitreal therapies must not damage retinal structure and function, and our results demonstrate that intravitreal PF4 administration (0.3 µg/eye) is well tolerated. Specifically, (1) OCT imaging showed well -preserved retinal morphology and thickness (Fig. 8A,B); (2) ERG revealed no significant changes in a-wave (photoreceptor function) or b-wave (inner retinal function) amplitudes (Fig. 8C,D); (3) histological examination confirmed retinal structural integrity (Fig. 8E); and (4) TUNEL staining showed no detectable cell apoptosis (Fig. 8F). This retinal toxicity profile, combined with its efficacy in preclinical models, suggests that PF4 may be a promising candidate for translation to human trials. Future studies are needed to define its long-term safety, optimize delivery, and determine its potential synergy with existing anti-VEGF treatments in clinically relevant settings.

5. Limitations

This study provides a preclinical proof-of-concept validating the therapeutic potential of PF4 for CNV. However, several limitations should be acknowledged when interpreting our findings, and addressing these gaps will be essential to advance PF4 from a therapeutic concept to a viable drug candidate.

First, while the laser-induced CNV model is a standard for testing anti-angiogenic therapies, it is fundamentally a wound-healing model triggered by acute thermal injury, which differs from the chronic, multifactorial process of human age-related macular degeneration (AMD). Second, due to technical constraints in sampling the minute vitreous volume in mice, a precise intraocular pharmacokinetic (PK) profile for exogenous PF4 was not established. Future studies in larger animal models, such as rabbits, are required to accurately map its clearance dynamics. Furthermore, while our 7-day assessments demonstrated a favorable retinal safety profile, the long-term effects and potential immunogenicity (e.g., anti-drug antibodies) of repeated dosing must be rigorously evaluated in future translational studies. Third, although we frame PF4 as a potential complementary agent to existing anti-VEGF therapies, this study did not include direct head-to-head comparisons or combination studies with anti-VEGF agents. Such studies will be essential to establish its relative efficacy and potential synergistic benefits. Finally, although we characterized the tissue-level localization of PF4, its precise subcellular trafficking following intravitreal injection requires further investigation. Addressing these gaps in future studies will be essential for translating PF4 toward clinical application.

6. Conclusions

In conclusion, intravitreal PF4 markedly reduced neovascular lesion formation and vascular leakage in the laser-induced CNV model, while attenuating retinal inflammatory responses, decreasing VEGFA and total VEGFR2 expression, and suppressing ERK/STAT3 activation, with good structural and functional tolerability in the eye. In addition, PF4 reduced PRNV in Vldlr$^{-/-}$ mice, providing complementary *in vivo* support for its anti-angiogenic activity. *In vitro*, PF4 inhibited VEGF-induced angiogenic behaviors of HRMECs (proliferation, migration, and tube formation) and reduced VEGF-triggered AKT/ERK/STAT3 phosphorylation. Together, these findings demonstrate that PF4 exerts both anti-angiogenic and anti-inflammatory effects in preclinical models, supporting further investigation of PF4 for the treatment of nAMD and related neovascular retinal diseases.

Abbreviations

nAMD, neovascular age-related macular degeneration; CNV, choroidal neovascularization; PF4, platelet factor 4; VEGF, vascular endothelial growth factor; VEGFA, vascular endothelial growth factor A; VEGFR2, vascular endothelial growth factor receptor 2; ERK, extracellular signal-regulated kinase; STAT3, signal transducer and activator of transcription 3; AKT, protein kinase B; HRMECs, human retinal microvascular endothelial cells; Vldlr$^{-/-}$, very low-density lipoprotein receptor knockout.

Availability of Data and Materials

All data reported in this paper will also be shared by the lead contact upon request.

Author Contributions

XK was the primary lead for experiments and data collection and drafted the original manuscript. SLiang, TQ, SLi, JL, and HH participated in data collection. XW, SH, DZ, and HY contributed to overall study conception and top-level design. YG provided key input on study conceptualization (including defining experimental groups) and interpreted histological data; MX designed critical experimental protocols and analyzed and interpreted molecular data; ML developed the detailed methodological framework and analyzed and interpreted functional outcomes. YG, MX, ML, and HY critically reviewed the manuscript and provided final manuscript oversight. HY also secured funding. All authors contributed to editorial changes in the manuscript, read and approved the final version of the manuscript for publication, and all authors have participated sufficiently in the work and agreed to be accountable for all aspects of the work.

Ethics Approval and Consent to Participate

All animal procedures were approved by the Institutional Animal Care and Use Committee of Tianjin Medical University (TMUaMEC 2024030) and conformed to the ARVO Statement for the Use of Animals in Ophthalmic and Vision Research, as well as the ARRIVE guidelines.

Acknowledgment

The authors thank the clinical and research staff at Tianjin Medical University General Hospital and Tianjin Medical University for their valuable assistance with data collection and technical support.

Funding

This work is supported by grants from the National Natural Science Foundation of China (82530032, 82330031) to HY, the National Natural Science Foundation of China (82401296) to ML, the Natural Science Foundation of Tianjin (25JCZDJC00390) to HY, the Natural Science Foundation of Tianjin (25JCQNJC00680) to ML, the Natural Science Foundation of Tianjin (23JCQNJC01180) to HH, and the Tianjin Key Medical Discipline Construction Project (NO. TJYXZDXK-3-004A) to HY.

Conflict of Interest

The authors declare no conflict of interest. Given his role as the Editorial Board member, Shikun He had no involvement in the peer-review of this article and has no access to information regarding its peer review. Full responsibility for the editorial process for this article was delegated to Dario Rusciano.

Declaration of AI and AI-Assisted Technologies in the Writing Process

During the preparation of this work the authors used ChatGPT-3.5 in order to check spell and grammar. After using this tool, the authors reviewed and edited the content as needed and takes full responsibility for the content of the publication.

References

[1] Wong WL, Su X, Li X, Cheung CMG, Klein R, Cheng CY, *et al*. Global prevalence of age-related macular degeneration and disease burden projection for 2020 and 2040: a systematic review and meta-analysis. The Lancet. Global Health. 2014; 2: e106–e116. https://doi.org/10.1016/S2214-109X(13)70145-1.

[2] Kim J, Mirando AC, Popel AS, Green JJ. Gene delivery nanoparticles to modulate angiogenesis. Advanced Drug Delivery Reviews. 2017; 119: 20–43. https://doi.org/10.1016/j.addr.2016.11.003.

[3] Guymer RH, Campbell TG. Age-related macular degeneration. Lancet (London, England). 2023; 401: 1459–1472. https://doi.org/10.1016/S0140-6736(22)02609-5.

[4] Fleckenstein M, Schmitz-Valckenberg S, Chakravarthy U. Age-Related Macular Degeneration: A Review. JAMA. 2024; 331: 147–157. https://doi.org/10.1001/jama.2023.26074.

[5] Kim J, Lee YJ, Won JY. Molecular Mechanisms of Retinal Pigment Epithelium Dysfunction in Age-Related Macular Degeneration. International Journal of Molecular Sciences. 2021; 22: 12298. https://doi.org/10.3390/ijms222212298.

[6] Song D, Liu P, Shang K, Ma Y. Application and mechanism of anti-VEGF drugs in age-related macular degeneration. Frontiers in Bioengineering and Biotechnology. 2022; 10: 943915. https://doi.org/10.3389/fbioe.2022.943915.

[7] Bai Y, Wang X, Qi F, Zuo X, Zou G. Mechanisms of action of retinal microglia in diabetic retinopathy (Review). International Journal of Molecular Medicine. 2025; 56: 202. https://doi.org/10.3892/ijmm.2025.5643.

[8] Fu X, Feng S, Qin H, Yan L, Zheng C, Yao K. Microglia: The breakthrough to treat neovascularization and repair blood-retinal barrier in retinopathy. Frontiers in Molecular Neuroscience. 2023; 16: 1100254. https://doi.org/10.3389/fnmol.2023.1100254.

[9] Fan W, Huang W, Chen J, Li N, Mao L, Hou S. Retinal microglia: Functions and diseases. Immunology. 2022; 166: 268–286. https://doi.org/10.1111/imm.13479.

[10] Comparison of Age-related Macular Degeneration Treatments Trials (CATT) Research Group, Maguire MG, Martin DF, Ying GS, Jaffe GJ, Daniel E, *et al*. Five-Year Outcomes with Anti-Vascular Endothelial Growth Factor Treatment of Neovascular Age-Related Macular Degeneration: The Comparison of Age-

Related Macular Degeneration Treatments Trials. Ophthalmology. 2016; 123: 1751–1761. https://doi.org/10.1016/j.ophtha.2016.03.045.

[11] Comparison of Age-related Macular Degeneration Treatments Trials (CATT) Research Group, Martin DF, Maguire MG, Fine SL, Ying GS, Jaffe GJ, *et al*. Ranibizumab and bevacizumab for treatment of neovascular age-related macular degeneration: two-year results. Ophthalmology. 2012; 119: 1388–1398. https://doi.org/10.1016/j.ophtha.2012.03.053.

[12] Ying GS, Kim BJ, Maguire MG, Huang J, Daniel E, Jaffe GJ, *et al*. Sustained visual acuity loss in the comparison of age-related macular degeneration treatments trials. JAMA Ophthalmology. 2014; 132: 915–921. https://doi.org/10.1001/jamaophthalmol.2014.1019.

[13] Mettu PS, Allingham MJ, Cousins SW. Incomplete response to Anti-VEGF therapy in neovascular AMD: Exploring disease mechanisms and therapeutic opportunities. Progress in Retinal and Eye Research. 2021; 82: 100906. https://doi.org/10.1016/j.preteyeres.2020.100906.

[14] Muniyandi A, Hartman GD, Song Y, Mijit M, Kelley MR, Corson TW. Beyond VEGF: Targeting Inflammation and Other Pathways for Treatment of Retinal Disease. The Journal of Pharmacology and Experimental Therapeutics. 2023; 386: 15–25. https://doi.org/10.1124/jpet.122.001563.

[15] Warkentin TE. Platelet-activating anti-PF4 disorders: An overview. Seminars in Hematology. 2022; 59: 59–71. https://doi.org/10.1053/j.seminhematol.2022.02.005.

[16] Liu Z, Li L, Zhang H, Pang X, Qiu Z, Xiang Q, *et al*. Platelet factor 4(PF4) and its multiple roles in diseases. Blood Reviews. 2024; 64: 101155. https://doi.org/10.1016/j.blre.2023.101155.

[17] Maione TE, Gray GS, Petro J, Hunt AJ, Donner AL, Bauer SI, *et al*. Inhibition of angiogenesis by recombinant human platelet factor-4 and related peptides. Science (New York, N.Y.). 1990; 247: 77–79. https://doi.org/10.1126/science.1688470.

[18] Jouan V, Canron X, Alemany M, Caen JP, Quentin G, Plouet J, *et al*. Inhibition of in vitro angiogenesis by platelet factor-4-derived peptides and mechanism of action. Blood. 1999; 94: 984–993.

[19] Leiter O, Brici D, Fletcher SJ, Yong XLH, Widagdo J, Matigian N, *et al*. Platelet-derived exerkine CXCL4/platelet factor 4 rejuvenates hippocampal neurogenesis and restores cognitive function in aged mice. Nature Communications. 2023; 14: 4375. https://doi.org/10.1038/s41467-023-39873-9.

[20] Zhang D, Hu F, Li T, Liu H, Li Q, Cheng Y, *et al*. Platelet factor 4 attenuates inflammation of microglia and protects retinal ganglion cells in retinal excitotoxicity. Experimental Eye Research. 2025; 255: 110352. https://doi.org/10.1016/j.exer.2025.110352.

[21] Lambert V, Lecomte J, Hansen S, Blacher S, Gonzalez MLA, Struman I, *et al*. Laser-induced choroidal neovascularization model to study age-related macular degeneration in mice. Nature Protocols. 2013; 8: 2197–2211. https://doi.org/10.1038/nprot.2013.135.

[22] Cai S, Yang Q, Cao Y, Li Y, Liu J, Wang J, *et al*. PF4 antagonizes retinal neovascularization via inhibiting PRAS40 phosphorylation in a mouse model of oxygen-induced retinopathy. Biochimica et Biophysica Acta. Molecular Basis of Disease. 2020; 1866: 165604. https://doi.org/10.1016/j.bbadis.2019.165604.

[23] Cui B, Guo X, Zhou W, Zhang X, He K, Bai T, *et al*. Exercise alleviates neovascular age-related macular degeneration by inhibiting AIM2 inflammasome in myeloid cells. Metabolism: Clinical and Experimental. 2023; 144: 155584. https://doi.org/10.1016/j.metabol.2023.155584.

[24] Bai T, Cui B, Xing M, Chen S, Zhu Y, Lin D, *et al*. Stable inhibition of choroidal neovascularization by adeno-associated virus 2/8-vectored bispecific molecules. Gene Therapy. 2024; 31: 511–523. https://doi.org/10.1038/s41434-024-00461-1.

[25] Liu S, Xiang K, Lei Q, Qiu S, Xiang M, Jin K. An optimized procedure to record visual evoked potential in mice. Experimental Eye Research. 2022; 218: 109011. https://doi.org/10.1016/j.exer.2022.109011.

[26] Sun Y, Lin Z, Liu CH, Gong Y, Liegl R, Fredrick TW, *et al*. Inflammatory signals from photoreceptor modulate pathological retinal angiogenesis via c-Fos. The Journal of Experimental Medicine. 2017; 214: 1753–1767. https://doi.org/10.1084/jem.20161645.

[27] Xu Y, Huang S, Zhou S, Wang X, Wei M, Chen X, *et al*. Iron Chelator Deferiprone Restores Iron Homeostasis and Inhibits Retinal Neovascularization in Experimental Neovascular Age-Related Macular Degeneration. Investigative Ophthalmology & Visual Science. 2024; 65: 5. https://doi.org/10.1167/iovs.65.10.5.

[28] Wang H, Han X, Wittchen ES, Hartnett ME. TNF-α mediates choroidal neovascularization by upregulating VEGF expression in RPE through ROS-dependent β-catenin activation. Molecular Vision. 2016; 22: 116–128.

[29] Nagineni CN, Kommineni VK, William A, Detrick B, Hooks JJ. Regulation of VEGF expression in human retinal cells by cytokines: implications for the role of inflammation in age-related macular degeneration. Journal of Cellular Physiology. 2012; 227: 116–126. https://doi.org/10.1002/jcp.22708.

[30] Sakurai E, Anand A, Ambati BK, van Rooijen N, Ambati J. Macrophage depletion inhibits experimental choroidal neovascularization. Investigative Ophthalmology & Visual Science. 2003; 44: 3578–3585. https://doi.org/10.1167/iovs.03-0097.

[31] Tsutsumi C, Sonoda KH, Egashira K, Qiao H, Hisatomi T, Nakao S, *et al*. The critical role of ocular-infiltrating macrophages in the development of choroidal neovascularization. Journal of Leukocyte Biology. 2003; 74: 25–32. https://doi.org/10.1189/jlb.0902436.

[32] Ramanathan M, Pinhal-Enfield G, Hao I, Leibovich SJ. Synergistic up-regulation of vascular endothelial growth factor (VEGF) expression in macrophages by adenosine A2A receptor agonists and endotoxin involves transcriptional regulation via the hypoxia response element in the VEGF promoter. Molecular Biology of the Cell. 2007; 18: 14–23. https://doi.org/10.1091/mbc.e06-07-0596.

[33] Heloterä H, Kaarniranta K. A Linkage between Angiogenesis and Inflammation in Neovascular Age-Related Macular Degeneration. Cells. 2022; 11: 3453. https://doi.org/10.3390/cells11213453.

[34] Fu Z, Liegl R, Wang Z, Gong Y, Liu CH, Sun Y, *et al*. Adiponectin Mediates Dietary Omega-3 Long-Chain Polyunsaturated Fatty Acid Protection Against Choroidal Neovascularization in Mice. Investigative Ophthalmology & Visual Science. 2017; 58: 3862–3870. https://doi.org/10.1167/iovs.17-21796.

[35] Wang X, Huang J, Fan W, Li N, Yang H, Yang W, *et al*. Lactate-binding protein DNMT3A in HRMECs promotes angiogenesis by upregulating VEGFA through HIF-1α lactylation. Genome Biology. 2025; 26: 377. https://doi.org/10.1186/s13059-025-03845-7.

[36] Ang KH, Thura M, Tan QSW, Gupta A, Kuan KY, Li J, *et al*. PRL3-zumab as an anti-angiogenic therapy in neovascular eye diseases. Nature Communications. 2025; 16: 4791. https://doi.org/10.1038/s41467-025-59929-2.

[37] Zhang J, Mao K, Gu Q, Wu X. The Antiangiogenic Effect of Sanguinarine Chloride on Experimental Choroidal Neovacularization in Mice via Inhibiting Vascular Endothelial Growth Factor. Frontiers in Pharmacology. 2021; 12: 638215. https://doi.org/10.3389/fphar.2021.638215.

[38] Pérez-Gutiérrez L, Ferrara N. Biology and therapeutic targeting of vascular endothelial growth factor A. Nature Reviews. Molecular Cell Biology. 2023; 24: 816–834. https://doi.org/10.1038/s41580-023-00631-w.

[39] Liu Y, Tang J, Wei P, Yu Z, Wu Z, Zhao X, *et al*. Microglial HMOX1 drives retinal angiogenesis via modulation of endothelial STAT3 signaling. Free Radical Biology & Medicine. 2026; 243: 29–42. https://doi.org/10.1016/j.freeradbiomed.2025.11.018.

[40] Yang L, Du J, Hou J, Jiang H, Zou J. Platelet factor-4 and its p17-70 peptide inhibit myeloma proliferation and angiogenesis in vivo. BMC Cancer. 2011; 11: 261. https://doi.org/10.1186/1471-2407-11-261.

[41] Bakogiannis C, Sachse M, Stamatelopoulos K, Stellos K. Platelet-derived chemokines in inflammation and atherosclerosis. Cytokine. 2019; 122: 154157. https://doi.org/10.1016/j.cyto.2017.09.013.

[42] Joyal JS, Sun Y, Gantner ML, Shao Z, Evans LP, Saba N, *et al*. Retinal lipid and glucose metabolism dictates angiogenesis through the lipid sensor Ffar1. Nature Medicine. 2016; 22: 439–445. https://doi.org/10.1038/nm.4059.

[43] Kuppermann BD, Goldstein M, Maturi RK, Pollack A, Singer M, Tufail A, *et al*. Dexamethasone Intravitreal Implant as Adjunctive Therapy to Ranibizumab in Neovascular Age-Related Macular Degeneration: A Multicenter Randomized Controlled Trial. Ophthalmologica. Journal International D'ophtalmologie. International Journal of Ophthalmology. Zeitschrift Fur Augenheilkunde. 2015; 234: 40–54. https://doi.org/10.1159/000381865.

[44] Todorich B, Thanos A, Yonekawa Y, Mane G, Hasbrook M, Thomas BJ, *et al*. Simultaneous dexamethasone intravitreal implant and anti-VEGF therapy for neovascular age-related macular degeneration resistant to anti-VEGF monotherapy. Journal of Vitreoretinal Diseases. 2017; 1: 65–74. https://doi.org/10.1177/2474126416683299.

[45] Gengrinovitch S, Greenberg SM, Cohen T, Gitay-Goren H, Rockwell P, Maione TE, *et al*. Platelet factor-4 inhibits the mitogenic activity of VEGF121 and VEGF165 using several concurrent mechanisms. The Journal of Biological Chemistry. 1995; 270: 15059–15065. https://doi.org/10.1074/jbc.270.25.15059.

[46] Lasagni L, Francalanci M, Annunziato F, Lazzeri E, Giannini S, Cosmi L, *et al*. An alternatively spliced variant of CXCR3 mediates the inhibition of endothelial cell growth induced by IP-10, Mig, and I-TAC, and acts as functional receptor for platelet factor 4. The Journal of Experimental Medicine. 2003; 197: 1537–1549. https://doi.org/10.1084/jem.20021897.